

An Improved Method for Fitting p -Mode Profile Asymmetries

Bradley W. Hindman

*JILA and Department of Astrophysical and Planetary Sciences, University of Colorado,
Boulder, CO 80309-0440, USA*

hindman@solarz.colorado.edu

ABSTRACT

In a power spectrum of the Sun’s acoustic waves, the p modes have distinctly skewed frequency profiles. Furthermore, the asymmetry is observed to have the opposite sign in power spectra made from line-of-sight velocity and continuum intensity. The asymmetry and its reversal in sign has previously been explained using a combination of mechanisms that involve the acoustic source. A localized acoustic source within an acoustic cavity naturally generates asymmetric profiles through wave interference; however, the sign of the asymmetry due to this mechanism is identical for all observables. The reversal of the asymmetry between velocity and intensity observations has been attributed to the visibility of the source itself (i.e., “correlated noise”). In this paper, I will show that asymmetry generated by a localized source can be interpreted as either a wave interference effect in physical space, or a mode interference effect in spectral space. I advocate a new mode-fitting procedure based on this new interpretation, whereby the complex phases of all the modes determine the mode asymmetries. Further, I suggest that information about the acoustic source function is encapsulated in the amplitude of each mode, and present a scheme by which the source function can be obtained from measured mode amplitudes by standard helioseismic inversion techniques.

Subject headings: Methods: data analysis—Sun: helioseismology—Sun: oscillations—Waves

1. Introduction

In power spectra of solar acoustic oscillations the frequency profiles of the p modes are skewed and markedly non-Lorentzian. This property was first discovered using Ca II K observations made from the geographic South Pole (Duvall et al. 1993) and were later

confirmed (Nigam & Kosovichev 1998) with modern spacecraft-based telescopes using data from the Michelson Doppler Imager (MDI) onboard the Solar and Heliospheric Observatory (SOHO). In both sets of observations, a puzzling fact was revealed: for modes of the same frequency and harmonic degree, the asymmetry or skewness of the line profile has opposite signs for observations made in the continuum intensity and line-of-sight Doppler velocity. For both types of observations, the lowest-frequency modes are the most severely skewed and the asymmetry appears to be only a weak function of harmonic degree; however, for modes of high harmonic degree ($l \gtrsim 150$) this statement is difficult to verify because the mode peaks are highly blended with the spatial leaks from modes of nearby degree, forming a broad ridge of power. Figures 1 and 2 illustrate the asymmetry for both high and low degree. From the figures it is evident that the frequency profile of each individual mode is asymmetric and, at high degree, the blended ridge is also asymmetric.

The physical mechanism for this skewness depends somewhat on whether we are considering the asymmetry of each mode profile or the asymmetry of a blended ridge. In the former case, the asymmetry of each mode is now thought to arise from a combination of effects due to the nature and location of the acoustic wave source. At high harmonic degree, the asymmetry of the p mode ridge is the result of the skewness of each component mode profile as well as an uneven distribution of power amongst the spatial leaks. The wave source can introduce skewness in a variety of ways. The first mechanism that I discuss here relies in detail on the location of the acoustic source. The primary source of acoustic waves in the Sun is granular convection. Short-lived convective events of relatively high Mach number prolifically emit sound waves. Since granulation is confined to a narrow band just below the photosphere, the acoustic source is highly localized in depth. Waves generated in this layer propagate both upwards and downwards. Those that propagate downwards are eventually refracted back upwards at the bottom of the acoustic cavity by the sound speed gradient. When this initially downward propagating wave returns to the excitation layer, it can destructively interfere with the wave that was initially upward propagating. At particular frequencies, complete destructive interference occurs and zero wave amplitude is observed above the excitation layer (which is where the spectral lines used in actual observations are formed). The frequencies at which the interference is complete are asymmetrically placed between the mode ridges, thereby leading to asymmetric mode profiles (Gabriel 1992, 1995; Roxburgh & Vorontsov 1995; Abrams & Kumar 1996; Rast & Bogdan 1998).

The second mechanism due to the source arises because the convective events that generate sound waves are themselves regions of intense temperature fluctuation and high velocity. The sources therefore provide a contribution to the power in either intensity or velocity observations. Since the acoustic waves are correlated with the source that generates them, the visibility of the source can lead to power that varies significantly over the line

profile and cause skewness. This mechanism has been dubbed “correlated noise” and has been suggested as the reason why the asymmetry is opposite for intensity and velocity spectra (Roxburgh & Vorontsov 1997; Nigam & Kosovichev 1998; Nigam et al. 1998). The current understanding is that in order to reproduce the asymmetry of both intensity and velocity power spectra and to explain the rapid variation with frequency of the phase of the cross-spectra between intensity and velocity (Oliviero et al. 1999), correlated noise must provide significant power to both types of spectra (e.g., Nigam et al. 1999; Skartlien & Rast 2000; Jefferies et al. 2003).

Numerical simulations of granulation have provided a counter explanation (Georgobiani et al. 2003). In these simulations, the velocity and intensity fluctuations have power spectra with asymmetric mode profiles. However, if the two quantities are sampled at the same geometric height the sign of the asymmetries are identical. Only after artificial Dopplergrams and intensity images have been constructed using radiative transfer do the two types of power spectra exhibit opposite asymmetries. Therefore, these simulations suggest that details of the radiative transfer, such as the different heights at which the two observables are formed and the nonlinear interaction between wave fluctuations and the radiation field, are responsible for the opposite skewnesses.

Unfortunately, many mode-fitting schemes used to measure p mode frequencies assume that the line profile is symmetric, a Lorentzian in fact. Duvall et al. (1993) estimate that failing to account for the asymmetry in the mode’s frequency profile can lead to mismeasurement of mode frequencies by as much as one part in 10^4 , a significant error for the purposes of helioseismic inversions. This is probably the source of the systematic offset ($\sim 0.1 \mu\text{Hz}$) that was observed between frequencies obtained from intensity and velocity spectra (Toutain et al. 1997). To account for such systematic shifts, researchers have suggested a variety of asymmetric model profiles with which to fit the observations (e.g., Duvall et al. 1993; Nigam et al. 1998; Rosenthal 1998). Due to its practicality, the formulation of Nigam et al. (1998) is probably the most widely used, having been adapted for both the measurement of global mode frequencies (Toutain et al. 1998; Reiter et al. 2002; Korzennik 2005) and the fitting of ring-analysis spectra (Basu & Antia 1999; Basu et al. 2001; Tripathy et al. 2009). In essence, the profile of Nigam et al. (1998) is a Lorentzian times a polynomial in frequency, where the polynomial has been calculated by performing a low order expansion about the mode frequency ω_0 ,

$$P(\omega) = \frac{A}{1+x^2} [s^2 + (1+sx)^2] , \quad (1.1)$$

$$x \equiv (\omega - \omega_0)/\gamma . \quad (1.2)$$

In this formula, γ is the linewidth, A is the power amplitude, and s is an asymmetry parameter.

This expression is formally valid under fairly limited conditions. For example, it has been derived as a small argument expansion in terms of sx , which requires that asymmetry is weak and more restrictively that we confine our attention to the core of the line and avoid the wings. One clear sign of this restriction is that the profile isn't integrable, and does not contain a finite amount of energy. Second, it ignores the presence of nearby modes which may contribute to the power. This is a particularly onerous assumption for high degree modes for which the line widths are sufficiently large that the mode and the neighboring spatial leaks blend into a ridge. Figure 1 illustrates this later point quite well. Each ridge is a blending of mode peaks and the ridges are wide enough that they have begun to overlap.

Our goal here is to generate a fitting function that takes the skewness of the p -mode frequency profiles into account while maintaining its validity over a wide range of conditions. I do so by using a modal expansion of the wavefield to represent the power spectra using a small number of free parameters. This expansion is accomplished in a general manner that doesn't depend on details of the atmosphere or the mechanisms for wave damping and excitation. In the next section, Section 2, I discuss the driving and damping of acoustic p mode oscillations in broad terms. In Section 3, I derive the modal expansion of the wave field and compute the resulting power spectrum. In Section 4, I promulgate a fitting profile of the spectrum that treats the asymmetry as a mode interference phenomenon. Finally, in Section 5, I discuss my findings and suggests ways in which properties of the acoustic source could be deduced through inversion of the fitted complex mode amplitudes.

2. Driven Acoustic Oscillations

To avoid unnecessary complexity, consider a neutrally-stable, plane-parallel atmosphere—a reasonable approximation for modes of intermediate degree and larger ($l \gtrsim 20$) which are trapped within the solar convection zone. Acoustic waves in such an atmosphere obey the following wave equation:

$$\left[\nabla^2 - \frac{1}{c^2} \left(\frac{\partial^2}{\partial t^2} + 2\gamma \frac{\partial}{\partial t} + \omega_c^2 \right) \right] \psi(\mathbf{x}, t) = S(\mathbf{x}, t), \quad (2.1)$$

where the sound speed c and acoustic cut-off frequency ω_c are functions of height z . Technically, the damping rate γ may also vary with height, but for simplicity I will restrict my attention to a constant damping rate. The quantity ψ can represent any wave variable (with

a suitable definition for the acoustic cut-off frequency); however, in order to relate our findings to observed power spectra made from Dopplergrams, I will treat ψ as proportional to the vertical component of the velocity. The function $S(\mathbf{x}, t)$ represents the density of acoustic sources.

Since the atmosphere is invariant in the horizontal direction and in time, Equation (2.1) can be Fourier transformed trivially to obtain an ODE in only the height coordinate z ,

$$\left[\frac{d^2}{dz^2} + \frac{\Omega^2(\omega)}{c^2(z)} - V(z; k) \right] \psi(z; \mathbf{k}, \omega) = S(z; \mathbf{k}, \omega) , \quad (2.2)$$

where I adopt several definitions,

$$\Omega^2(\omega) \equiv \omega^2 + 2i\gamma\omega , \quad (2.3)$$

$$V(z; k) \equiv \frac{\omega_c^2(z)}{c^2(z)} - k^2 , \quad (2.4)$$

and use the following Fourier convention:

$$\phi(\mathbf{k}, \omega) = \int_{-\infty}^{\infty} \int_{-\infty}^{\infty} \int_{-\infty}^{\infty} dx dy dt \phi(\mathbf{x}, t) e^{-i(k_x x + k_y y - \omega t)} , \quad (2.5)$$

$$\phi(\mathbf{x}, t) = \frac{1}{(2\pi)^3} \int_{-\infty}^{\infty} \int_{-\infty}^{\infty} \int_{-\infty}^{\infty} dk_x dk_y d\omega \phi(\mathbf{k}, \omega) e^{i(k_x x + k_y y - \omega t)} . \quad (2.6)$$

The frequency Ω is inherently complex and the acoustic potential V is purely real. Note, that if the complex wave frequency $\omega = \omega_r + i\omega_i$ has an imaginary part $\omega_i = -\gamma$, then the frequency Ω is purely real with $\Omega = \sqrt{\omega_r^2 + \gamma^2}$. This allows the solution to the damped problem to be generated by solving an equivalent undamped problem and then shifting the resulting frequency, in both its real and imaginary components, by an amount dependent on the damping rate, $\omega = \sqrt{\Omega^2 - \gamma^2} - i\gamma$.

2.1. Green's Function

I commence by solving for the spectral Green's function G . For a point source located at the height z' , the Green's function satisfies

$$\left[\frac{d^2}{dr^2} + \frac{\Omega^2}{c^2} - V \right] G(z, z'; k, \omega) = \delta(z - z') . \quad (2.7)$$

The Green's function can be found in the standard way. If I denote ψ_- as the homogeneous solution that obeys the boundary conditions deep in the atmosphere (as $z \rightarrow -\infty$) and similarly write ψ_+ as the homogeneous solution that obeys the boundary condition high in the atmosphere (as $z \rightarrow +\infty$), the Green's function may be written in the following form:

$$G(z, z'; k, \omega) = \frac{\Psi(z, z'; k, \omega)}{\mathcal{W}(k, \omega)} , \quad (2.8)$$

where \mathcal{W} is the Wronskian of the two homogeneous solutions and Ψ is their product,

$$\mathcal{W}(k, \omega) \equiv \psi_- \frac{d\psi_+}{dz} - \frac{d\psi_-}{dz} \psi_+ , \quad (2.9)$$

$$\Psi(z, z'; k, \omega) \equiv \begin{cases} \psi_-(z; k, \omega) \psi_+(z'; k, \omega) & \text{if } z < z' \\ \psi_-(z'; k, \omega) \psi_+(z; k, \omega) & \text{if } z > z' . \end{cases} \quad (2.10)$$

Equation (2.8) has been used extensively in the past to explain the asymmetry of the p -mode frequency profiles in the Sun's acoustic spectrum (Gabriel 1992; Roxburgh & Vorontsov 1995; Abrams & Kumar 1996; Rast & Bogdan 1998). Since the driving of acoustic waves is thought to arise from granulation, which is localized in a thin layer just below the photosphere, I make the assumption that the height dependence of the source function is in fact just a delta function,

$$S(z; \mathbf{k}, \omega) = \delta(z - z') S_0(\mathbf{k}, \omega) . \quad (2.11)$$

This means that the Green's function provides the correct vertical behavior of the full wavefield.

If one further assumes that the spectral line used to observe the wavefield forms at a height that overlies the driving layer ($z > z'$), the solution becomes

$$\psi(z; \mathbf{k}, \omega) = S_0(\mathbf{k}, \omega) \frac{\psi_-(z'; k, \omega) \psi_+(z; k, \omega)}{\mathcal{W}(k, \omega)} . \quad (2.12)$$

The power spectrum of such a wavefield, observed at a height z in the atmosphere, is of course

$$P(\mathbf{k}, \omega) = |\psi(z; \mathbf{k}, \omega)|^2 = |S_0(\mathbf{k}, \omega)|^2 \frac{|\psi_-(z'; k, \omega)|^2 |\psi_+(z; k, \omega)|^2}{|\mathcal{W}(k, \omega)|^2}, \quad (2.13)$$

which may be thought of as having four separate contributions: (1) the strength of the source $|S_0|^2$, (2) a contribution from the Wronskian $|\mathcal{W}|^{-2}$ that represents the modal structure of the acoustic cavity, (3) a contribution from the driving efficiency $|\psi_-(z'; k, \omega)|^2$, and (4) a contribution from the height of observation $|\psi_+(z; k, \omega)|^2$. The Wronskian possesses a zero at each mode frequency (which in the present formulation will be a complex frequency because of damping). These zeros generate Lorentzian peaks in the power spectrum at each mode frequency and by themselves these peaks are symmetric functions of frequency. The observed asymmetry arises from the driving efficiency which expresses how well the driver couples to any given mode. The driving efficiency possesses zeros wherever the homogeneous solution ψ_- has a node at the driving height. This occurs whenever the downward propagating wave generated by the source rebounds off the lower turning point of the acoustic cavity and returns to the driving layer with the exact phase needed to destructively interfere with the upward propagating wave also excited by the source. When this occurs, the solution vanishes for all heights above the driving layer. The zeroes in the driving efficiency fall in between the mode frequencies and are not distributed symmetrically about the mode peaks; hence, they generate asymmetry in the total power profile (for complete details see Rast & Bogdan 1998).

2.2. A Simple Example

To illustrate the salient features of this behavior without undue complications, consider a simple “guitar-string” model. Waves are trapped between two heights in the atmosphere, $z = 0$ and $z = L$, at which the solution ψ must vanish. Further, within this cavity let the sound speed be constant and let the acoustic potential vanish. The solutions are therefore purely sinusoidal with wavenumber $K = \Omega/c$,

$$\psi_-(z; \omega) = \sin(Kz), \quad (2.14)$$

$$\psi_+(z; \omega) = \sin[K(L - z)], \quad (2.15)$$

$$\mathcal{W}(\omega) = K \sin(KL). \quad (2.16)$$

If I assume that the driving height lies below the observation height, and further assume that the spectral dependence of the driver is white (i.e., S_0 is a constant function of frequency), then the power spectrum of the solution is as follows:

$$P(\omega) = |S_0|^2 \frac{\sin^2(Kz') \sin^2[K(L-z)]}{K^2 \sin^2(KL)}. \quad (2.17)$$

The frequency dependence of this expression is illustrated in Figure 3 with the thick black curve. The individual contributions from the Wronskian, $|K \sin(KL)|^{-2}$ (red curve), the driving efficiency, $\sin^2(Kz')$ (blue curve) and the observation height, $\sin^2[K(L-z)]$ (green curve), are also indicated. The line asymmetry arises because the spacing between the zeros in the driving efficiency is smaller than the spacing between modes (i.e., the spacing between the zeros of the Wronskian). The most asymmetric modes (those at low frequency) are those for which a zero in the driving efficiency almost coincides with a mode frequency. For the model presented in the figure, the height of observation is very close to the upper boundary of the acoustic cavity (as is true for helioseismic observations of solar p modes). This leads to a slow frequency variation in the power due to the height of formation; therefore, this term only provides a slow variation in the overall amplitude instead of skewness.

3. Modal Decomposition

While Equation (2.13) is useful for understanding why the Sun’s p -mode profiles are observed to be asymmetric functions of frequency, this formulation for the solution ψ and the resulting power spectrum P does not lend itself readily to the problem of mode fitting, whereby the mode parameters (i.e., frequency, lifetime and amplitude) are measured from an observed spectrum. Explicit use of Equation (2.13) requires prior knowledge of the homogeneous solutions ψ_- and ψ_+ which pre-supposes a detailed understanding of the structure of the solar atmosphere (obtaining such an understanding may be the reason that one is measuring the mode frequencies in the first place). A more natural representation of the solution would be a modal decomposition, where the mode parameters are represented explicitly.

If one ignores the existence of a global cut-off frequency and therefore neglects the possibility of leaky modes and continuous spectra, one may use the orthogonality properties of the eigenfunctions of the homogeneous problem,

$$\int_{-\infty}^{\infty} dz \frac{\psi_n(z; k) \psi_m(z; k)}{c^2(z)} = \delta_{nm}, \quad (3.1)$$

to perform a standard eigenfunction expansion of the solution, generating the following expression for the wavefield:

$$\psi(z; \mathbf{k}, \omega) = S_0(\mathbf{k}, \omega) \sum_{n=1}^{\infty} \frac{\psi_n(z'; k) \psi_n(z; k)}{\Omega^2 - \Omega_n^2(k)}. \quad (3.2)$$

When the atmosphere possesses a global cut-off frequency (as is true for the Sun's p modes), an eigenfunction expansion is still possible; however, the expressions are more complicated due to the existence of continuous spectra. To avoid obscuring the important issues with unneeded mathematics, I will consider such possibilities separately in Appendix A. In Equation (3.2) the eigenvalues Ω_n^2 and eigenfunctions ψ_n are purely real, whereas Ω^2 is complex. This formulation is completely equivalent to that shown previously in Equation (2.12); however, in this treatment the contribution from each mode to the power is explicitly represented,

$$P(\mathbf{k}, \omega) = |S_0(\mathbf{k}, \omega)|^2 \left| \sum_{n=1}^{\infty} \frac{\psi_n(z'; k) \psi_n(z; k)}{\Omega^2 - \Omega_n^2(k)} \right|^2. \quad (3.3)$$

Note that each eigenfunction ψ_n is associated with two separate complex eigenfrequencies $\omega_{\pm n}(k) = \pm \hat{\omega}_n(k) - i\gamma$, one with a positive real part (which I will denote with the positive index n) and one with a negative real part (denoted with the negative index $-n$). Therefore, the contribution from each eigenmode can be decomposed into its two frequency components,

$$\psi(z; \mathbf{k}, \omega) = S_0(\mathbf{k}, \omega) \sum_{n=1}^{\infty} \frac{\psi_n(z'; k) \psi_n(z; k)}{2\hat{\omega}_n(k)} \left\{ \frac{1}{\omega - \omega_n} - \frac{1}{\omega - \omega_{-n}} \right\}, \quad (3.4)$$

$$= S_0(\mathbf{k}, \omega) \sum_{n=-\infty}^{\infty} \frac{\psi_n(z'; k) \psi_n(z; k)}{2\hat{\omega}_n(k)} \frac{1 - \delta_{n0}}{\omega - \omega_n(k)}, \quad (3.5)$$

$$P(\mathbf{k}, \omega) = |S_0(\mathbf{k}, \omega)|^2 \left| \sum_{n=-\infty}^{\infty} \frac{\psi_n(z'; k) \psi_n(z; k)}{2\hat{\omega}_n(k)} \frac{1 - \delta_{n0}}{\omega - \omega_n(k)} \right|^2. \quad (3.6)$$

The summation over n now includes the negative indices, the variable $\hat{\omega}_n (= -\hat{\omega}_{-n})$ is the real part of the complex mode frequency, and the factor with the Kronecker delta δ_{n0} has been included to remove the $n = 0$ term from the summation.

The familiar representation of the power spectrum as the sum of modes, each with a Lorentzian profile, can be recovered by assuming that all of the modes are well-isolated from each other spectrally (the damping rate is much less than the spacing between modes). Therefore, mode interference cross-terms can be ignored and the power is just the incoherent sum of the power within each mode,

$$P_{\text{inc}}(\mathbf{k}, \omega) = |S_0(\mathbf{k}, \omega)|^2 \sum_{n \neq 0} \frac{|\psi_n(z'; k) \psi_n(z; k)|^2}{4\hat{\omega}_n^2(k)} \frac{1}{(\omega - \hat{\omega}_n)^2 + \gamma^2}. \quad (3.7)$$

Of course, each Lorentzian profile in Equation (3.7) is symmetric about the central mode frequency $\hat{\omega}_n(k)$. The asymmetry that is observed in p -mode line profiles comes from the mode interference terms that were neglected in Equation (3.7).

3.1. The Simple Example Revisited

The fact that interference between modes can be construed as the source of asymmetry in p -mode power profiles is aptly illustrated by the simple guitar-string model previously explored in Section 2.2. For this simple problem, the eigenvalues and eigenfunctions are defined by

$$\Omega_n = K_n c = \frac{n\pi c}{L}, \quad (3.8)$$

$$\omega_{\pm n} = \pm \hat{\omega}_n - i\gamma = \pm \sqrt{\Omega_n^2 - \gamma^2} - i\gamma, \quad (3.9)$$

$$\psi_n(z; \omega) = \left(\frac{2c^2}{L}\right)^{1/2} \sin(K_n z), \quad (3.10)$$

and the modal expansion is just a Fourier sine series,

$$\psi(z; \omega) = \frac{c^2 S_0}{L} \sum_{n \neq 0} \sin(n\pi z'/L) \sin(n\pi z/L) \frac{\hat{\omega}_n^{-1}}{\omega - \omega_n}, \quad (3.11)$$

$$P(\omega) = \frac{c^4 |S_0|^2}{L^2} \left| \sum_{n \neq 0} \sin(n\pi z'/L) \sin(n\pi z/L) \frac{\hat{\omega}_n^{-1}}{\omega - \omega_n} \right|^2. \quad (3.12)$$

The black curve in Figure 3 represents the power from either representation, equations (2.17) or (3.12). However, from the perspective of an eigenfunction expansion, the asymmetry in the frequency profile of each mode arises because of mode interference. Zeroes in the power are located at those frequencies for which complete destructive interference has occurred, where the interference in this interpretation is in spectral space between modes with overlapping power not in physical space between different wave components generated by the source.

Direct confirmation of this comes from plotting the incoherent sum of the power in all the modes,

$$P_{\text{inc}}(\omega) = \frac{c^4 |S_0|^2}{L^2} \sum_{n \neq 0} \sin^2(n\pi z'/L) \sin^2(n\pi z/L) \frac{\hat{\omega}_n^{-2}}{(\omega - \hat{\omega}_n)^2 + \gamma^2}. \quad (3.13)$$

In Figure 3 this sum is shown as the orange curve and it can clearly be seen that the frequency profiles are symmetric, albeit modified by a slowly varying background (which is formally composed of the wings of many modes).

4. Mode Fitting

In a traditional procedure, to measure properties of a p mode such as its frequency, amplitude and lifetime, the power within a narrow band of frequencies centered on the target mode is fit with a model function. The range of frequency is selected with the goal of mitigating the contamination from other modes. However, since spatial leakage produces spectral peaks that cannot be fully isolated from the target mode (see Figure 1), the fitting function is usually comprised of an incoherent sum of power peaks based on the properties of Equation (3.7). For the j th mode (where j indicates a particular combination of harmonic degree, azimuthal order and mode order) the fitting function might have the form,

$$P_{\text{model}}(\omega) = B(\omega) + \mathcal{P}_j(\omega) + \sum_{j'} C_{jj'} \mathcal{P}_{j'}(\omega) \quad (4.1)$$

where each profile $\mathcal{P}_j(\omega)$ is a Lorentzian function with three parameters,

$$\mathcal{P}_j(\omega) \equiv \frac{A_j}{(\omega - \hat{\omega}_j)^2 + \Gamma_j^2}. \quad (4.2)$$

In these expressions, B is a background function that represents incoherent solar noise, and the three parameters that describe the Lorentzian are its mode frequency $\hat{\omega}_j$, power amplitude A_j and line width Γ_j . The leakage is described by the leakage matrix $C_{jj'}$ and the summation is performed over all modes that have a frequency within the fitting window and that have significant leakage. All of the free parameters in this formulation are treated as real quantities.

Modern fitting procedures (e.g., Korzennik 2005) often attempt to account for the observed skewness in the mode profiles by using the asymmetric profile of Nigam et al. (1998),

Equation (1.1). Using the same notation presented here, Equation (1.1) becomes

$$\mathcal{P}_j(\omega) = \frac{A_j}{(\omega - \hat{\omega}_j)^2 + \Gamma_j^2} \left\{ s_j^2 + \left[1 + s_j \left(\frac{\omega - \hat{\omega}_j}{\Gamma_j} \right) \right]^2 \right\}, \quad (4.3)$$

which adds one additional parameter, the asymmetry parameter s_j , to each fitted peak.

As mentioned previously, this commonly used skewed Lorentzian function is only a valid representation within the core of the line and it does not include the effects of mode interference (in spectral space). Further, the energy contained by any given mode (and hence the amplitude parameter A_j) is poorly defined since each mode’s power profile lacks a finite integral. A globally valid expression that directly accounts for interference effects is suggested by the functional form of Equation (3.3),

$$P_{\text{model}}(\omega) = B(\omega) + \left| \frac{a_j}{\omega - \hat{\omega}_j + i\Gamma_j} + \sum_{j'} c_{jj'} \frac{a_{j'}}{\omega - \hat{\omega}_{j'} + i\Gamma_{j'}} \right|^2, \quad (4.4)$$

where the parameters all have the same meaning except that the mode amplitude a_j and the leakage matrix $c_{jj'}$ are now complex quantities. Unlike classical fitting functions, this model function properly captures asymmetric mode profiles in both the wing and core because the effects of mode interference are present through the retention of the cross-terms between modes. The cost of accounting for the asymmetry is the need to fit one additional parameter per mode, the complex phase of the amplitude $a_j = |a_j|e^{i\phi_j}$.

5. Discussion

I have suggested an alternate formula—Equation (4.4)—for fitting p -mode frequency profiles that is based on an eigenfunction expansion of the Green’s function. This formulation takes into account the skewness of the line profiles that is inherently produced by a localized acoustic source by including the effects of mode interference in spectral space. In addition, the fitting formula has the salutary features that it is valid for all frequencies across the mode profile (not just in the core of a line) and each mode contains a finite amount of energy.

The suggested scheme can be applied to the fitting of global modes of relatively low harmonic degree ($l \lesssim 200$) directly as envisioned. The asymmetry in a mode’s profile is primarily the result of interference with nearby spatial leaks, which are most likely from the same mode order or ridge (except at very low harmonic degree $l \lesssim 10$). On the other hand,

the proposed fitting model is not immediately relevant to the fitting of ring-analysis spectra. The asymmetry observed in the p -mode ridges at large harmonic degree ($l \gtrsim 200$) are not produced by the same mechanisms that generate the asymmetry for global modes. Instead, the asymmetry is largely a result of the spatial window function (the ring-analysis version of the blending of a mode and the nearby leaks).

Ring-analysis spectra are manufactured by Fourier transforming the wavefield observed on a small patch on the surface of the Sun. The small spatial domain translates into a broad spread of power in horizontal wavenumber. This widens the ridges and produces an effective line width that is much larger than one would expect based just on the mode lifetime. Furthermore, the resulting line profile depends on the window function applied during the Fourier analysis, the slope of the p -mode ridge in the dispersion diagram ($d\omega_n/dk$), and the variation in power along the ridge. Unlike in the global mode analyses where the effects of leakage have been considered in detail for over a decade, leakage has not been treated self-consistently in any ring-analysis studies. While the fitting formula presented here could be used to model the resulting ring-analysis spectra quite well with the asymmetry being produced by the interference between the ridges themselves, the underlying physical mechanism would be wrong. I leave it to a subsequent paper to include the effects of the leakage function on mode profiles.

5.1. Measuring the Acoustic Source Function

One novel property of the fitting function given by Equation (4.4) is that the effect of the source is directly represented by the complex mode amplitudes. Therefore, the additional parameters have a physical significance that can be used to ferret out information about acoustic sources and the convection that engenders them. This can be seen most easily if I relax the assumption that the source is proportional to a delta function in height. If instead the source is distributed, as usual the wavefield is obtained through a convolution of the Green's function with the source,

$$\psi(z; \mathbf{k}, \omega) = \sum_{n \neq 0} \frac{a_n(\mathbf{k}, \omega)}{\omega - \hat{\omega}_n(k)}, \quad (5.1)$$

$$= \sum_{n \neq 0} \int_{-\infty}^{\infty} dz' \frac{\psi_n(z'; k) \psi_n(z; k)}{2\hat{\omega}_n(k)} \frac{S(z'; \mathbf{k}, \omega)}{\omega - \omega_n(k)}. \quad (5.2)$$

Assuming that the source function is isotropic with a frequency variation that is slow com-

pared to the damping rate, the complex mode amplitude is therefore given by an integral over the source,

$$a_n(k) = \int_{-\infty}^{\infty} dz' \mathcal{K}_n(z'; k) S(z'; k, \omega_n), \quad (5.3)$$

$$\mathcal{K}_n(z'; k) \equiv \frac{\psi_n(z; k) \psi_n(z'; k)}{2\hat{\omega}_n(k)}, \quad (5.4)$$

where the set of \mathcal{K}_n are sensitivity kernels. Given a set of measured amplitudes, the coupled integral equations (5.3) could be inverted using standard helioseismic inversion procedures to obtain the source as a function of height in the atmosphere.

5.2. Effects of Correlated Noise

The theory and procedures that have been developed in this paper have so far ignored the existence of correlated noise. Previous studies have shown that correlated noise is a necessary ingredient to explain the reversal of asymmetry between Doppler-velocity spectra and continuum-intensity spectra (Roxburgh & Vorontsov 1997; Nigam & Kosovichev 1998; Nigam et al. 1998), as well as the rapid phase variation in velocity–intensity phase difference spectra (Skartlien & Rast 2000). The modal expansion presented here can easily be adapted to include the effects of correlated noise (e.g., Skartlien & Rast 2000); one simply adds a complex correlated noise component, ψ_{corr} , to the wavefield before computing the power,

$$P_{\text{model}}(\omega) = B(\omega) + \left| \frac{a_j}{\omega - \hat{\omega}_j + i\Gamma_j} + \sum_{j'} c_{jj'} \frac{a_{j'}}{\omega - \hat{\omega}_{j'} + i\Gamma_{j'}} + \psi_{\text{corr}} \right|^2, \quad (5.5)$$

Assuming that the correlated noise is due to the visibility of the source itself, one would expect that the phase and amplitude of the correlated noise ψ_{corr} would be a slowly varying function of frequency. Therefore, if one is fitting the power in a narrow frequency band, it can safely be assumed that the noise is a complex constant. Thus, in any fit to data the correlated noise adds only two additional parameters that must be fit. If one were fitting a broad range of frequencies, it might be necessary to parameterize the frequency dependence of the correlated noise. Since, the frequency variation should be rather weak, almost any smooth function with a only a few free parameters (polynomial, power law, gaussian, etc.) would probably work.

I thank Mark Rast for his help in understanding the effects of correlated noise. I thank Irene González-Hernández for providing the GONG data used to generate Figures 1 and 2. This work was supported by NASA through grants NNX08AJ08G, NNX08AQ28G, and NNX09AB04G.

A. Leaky Modes

The expansion of the wavefield into a discrete set of eigenmodes is appropriate only if the system lacks a continuous spectrum. Such spectra appear as branch cuts in the complex frequency plane. Here, I will consider two possible origins of such branch cuts. First, temporal damping of the form appearing in Equation (2.1) admits the possibility of overdamped solutions (OD). Such solutions manifest as a branch cut along the imaginary frequency axis. The existence of this branch cut is evident when one considers the frequency expression $\Omega = \sqrt{\omega^2 + 2i\gamma\omega}$. The square root function possesses branch points wherever its argument vanishes. Therefore, there are two branch points, one at $\omega = 0$ and the other at $\omega = -2i\gamma$, with a corresponding branch cut connecting them along the imaginary axis. Frequencies along this branch cut correspond to overdamped waves whose temporal dependence is pure decay without oscillation.

The second type of branch cut appears when the atmosphere possesses a global cut-off frequency, as the Sun does. If the product of the acoustic potential and the square of the sound speed remains bounded ($c^2V < \alpha^2$) as the height becomes large ($z \rightarrow \infty$), then waves of sufficiently large frequency ($\Omega > \alpha$) are not trapped and leaky waves (LW) which radiate to infinity become possible. In the Sun, the condition for leaky waves is $\omega/2\pi \gtrsim 5.2$ mHz. There are two branch points associated with such waves, each located in the lower half of the complex frequency plane where $\Omega^2 = \alpha^2$ or $\omega = \pm\sqrt{\alpha^2 - \gamma^2} - i\gamma$. I choose to connect these branch points separately to infinity as shown in Figure 4, and therefore the branch cut is bipartite. Frequencies along this branch cut correspond to propagating waves which radiate upwards through the photosphere, forming the high-frequency, pseudo-mode portion of the Sun’s acoustic spectrum.

When leaky waves are allowed by the boundary conditions, the system will not possess an infinite number of discrete eigenmodes. Instead, for a particular horizontal wavenumber k , the acoustic cavity will only have a finite number of discrete, trapped modes and a continuous spectrum of leaky modes. As before the trapped modes correspond to a zero in the Wronskian \mathcal{W} , or equivalently to a simple pole in the Green’s function. The leaky modes on the other hands correspond to the solutions along a branch cut. In an eigenfunction decomposition both types of waves are needed, as the discrete trapped waves on their own

do not form a complete set. For the problem at hand, these separate contributions can be calculated by Fourier transforms and contour integration in the complex frequency plane, which I perform in this appendix.

I begin by taking the inverse Fourier transform of the Green’s function as expressed in Equation (2.8),

$$\begin{aligned} G(z, z'; k, t) &= \frac{1}{2\pi} \int_{-\infty}^{\infty} d\omega G(z, z'; k, \omega) e^{-i\omega t} , \\ &= \frac{1}{2\pi} \int_C d\omega \frac{\Psi(r, r'; k, \omega)}{\mathcal{W}(k, \omega)} e^{-i\omega t} . \end{aligned} \quad (\text{A1})$$

The integral is a contour integral through the complex frequency plane along the contour C which lies initially along the real frequency axis—see Figure 4(a). Since all waves are damped, all of the poles and branch cuts appear in the lower half of the complex frequency plane. Therefore, for $t < 0$ one may freely deform the contour upward to infinity and the integrand will vanish exponentially for large imaginary frequency, leading to the conclusion $G = 0$. However, for $t > 0$, in order for the integrand to vanish once again as the contour is deformed to infinity, the deformation must be downwards into the lower half plane. Since the lower half plane contains the poles and branch cuts, the contour must be deformed around them and the integral acquires contributions from the integration around each singularity. Using the residue theorem to evaluate the integration around each pole, one obtains the contribution from each trapped mode,

$$\begin{aligned} G(z, z'; k, t) &= -i \sum_{n=-N}^N \frac{\psi_n(z'; k) \psi_n(z, k)}{\mathcal{W}'(k, \omega_n)} (1 - \delta_{n0}) H(t) e^{-i\omega_n t} \\ &\quad + \frac{1}{2\pi} \int_{C_{\text{BC}}} d\tilde{\omega} \frac{\Psi(z, z'; \tilde{\omega})}{\mathcal{W}(k, \tilde{\omega})} H(t) e^{-i\tilde{\omega} t} , \end{aligned} \quad (\text{A2})$$

where $H(t)$ is the Heaviside step function and the prime on the Wronskian denotes differentiation with respect to the frequency argument,

$$\mathcal{W}' \equiv \frac{d\mathcal{W}}{d\omega} . \quad (\text{A3})$$

Further, for future convenience, I have replaced the dummy variable of integration with $\tilde{\omega}$ and the integration contour is disjoint and surrounds all of the branch cuts $C_{\text{BC}} = C_{\text{OD}} + C_{\text{LW}}$. The summation over the index n is over a finite number ($2N$) of poles, which includes two poles per mode, one with a positive real part of the frequency and the other with a negative real part, $\omega_{\pm n} = \pm \hat{\omega}_n - i\gamma$. For clarity of notation, there is no pole associated with the index $n = 0$, and I have therefore included the factor with the Kronecker delta to exclude the $n = 0$ term from the summation.

Now that I have the Green's function in the form of an eigenfunction expansion, the result can be compared with Equation (3.2) by taking the temporal Fourier transform and including the effects of the source,

$$G(z, z'; k, \omega) = \sum_{n=-N}^N \frac{\psi_n(z'; k) \psi_n(z, k)}{\mathcal{W}'(k, \omega_n)} \frac{1 - \delta_{n0}}{\omega - \omega_n(k)} + \frac{1}{2\pi} \int_{C_{\text{BC}}} d\tilde{\omega} \frac{\Psi(z, z'; \tilde{\omega})}{\mathcal{W}(\tilde{\omega})} \frac{1}{\omega - \tilde{\omega}}, \quad (\text{A4})$$

$$\psi(z, z'; \mathbf{k}, \omega) = S_0(\mathbf{k}, \omega) \sum_{n=-N}^N \frac{\psi_n(z'; k) \psi_n(z, k)}{\mathcal{W}'(k, \omega_n(k))} \frac{1 - \delta_{n0}}{\omega - \omega_n} + \frac{S_0(\mathbf{k}, \omega)}{2\pi} \int_{C_{\text{BC}}} d\tilde{\omega} \frac{\Psi(z, z'; \tilde{\omega})}{\mathcal{W}(\tilde{\omega})} \frac{1}{\omega - \tilde{\omega}}. \quad (\text{A5})$$

In the equations above I have used the following Fourier transform identity,

$$\int_{-\infty}^{\infty} dt H(t) e^{i(\omega - \omega_n)t} = \frac{i}{\omega - \omega_n}. \quad (\text{A6})$$

One can easily verify that modulo the normalization of the eigenfunctions, Equation (A5) is equivalent to the modal expansion appearing in Section 3, Equation (3.5), except for the appearance of the integral around the branch cuts (continuous spectra of leaky waves) and a summation over only a finite number of trapped modes instead of a countable infinity.

Finally, note that due to the symmetries of the Wronskian \mathcal{W} and the function Ψ , the integral around the branch cut associated with overdamped waves can be shown by direct evaluation to vanish. This is true for any problem in which the overdamped waves are confined to a cavity of finite extent. In truly infinite domains the precise cancellation around

the contour does not occur and the overdamped solutions may play a role. Therefore, the contour integral need only include the spectrum of leaky waves, $C_{\text{BC}} = C_{\text{LW}}$.

A.1. Leaky Square-Well Potential

To illustrate the mathematics developed previously in this appendix, I extend the rudimentary guitar-string model presented in the main body of this paper. Instead of requiring that all waves reflect from the cavity boundaries, I will examine a square-well potential that permits high-frequency waves to escape out the top of the cavity. Consider a one-dimensional acoustic cavity of length L with constant sound speed and a global cut-off frequency. The acoustic potential $V(z)$ is identically zero within the cavity itself, and takes on a constant, nonzero value above the top of the cavity, $z > L$,

$$V(z) = \begin{cases} 0 & \text{if } z < L \\ \alpha^2/c^2 & \text{if } z > L. \end{cases} \quad (\text{A7})$$

At the lower boundary of the cavity, $z = 0$, the solution must vanish, and at the top of the cavity the solution must match smoothly onto either an evanescent solution (for $\Omega < \alpha$) or an upward travelling wave (for $\Omega > \alpha$). If I assume that the driving layer lies within the cavity itself ($z' < L$), the homogeneous solutions ψ_- and ψ_+ which obey the proper boundary conditions are as follows:

$$\psi_-(z; \omega) = \sin(Kz) \quad (\text{A8})$$

$$\psi_+(z; \omega) = \begin{cases} \cos[K(L-z)] + \kappa K^{-1} \sin[K(L-z)] & \text{if } z < L \\ \exp[-\kappa(z-L)] & \text{if } z > L, \end{cases} \quad (\text{A9})$$

where the constants K and κ are, respectively, the wavenumber within the cavity and the evanescence rate for the region above the cavity,

$$K(\omega) = \frac{\Omega(\omega)}{c}, \quad (\text{A10})$$

$$\kappa(\omega) = \frac{\sqrt{\alpha^2 - \Omega^2(\omega)}}{c}. \quad (\text{A11})$$

Note, if $\Omega^2 > \alpha^2$ the evanescence rate κ becomes purely imaginary. For frequencies lying on the top of the branch cut, I choose the sign of the square root in Equation (A11) such

that the imaginary part of κ is positive and the solution in the regime above the cavity, $z > L$, corresponds to an outward propagating wave and a radiation boundary condition is satisfied. Remember, the Fourier convention, Equation (2.6), is consistent with solutions with the time dependence $\sim e^{-i\omega t}$.

The Wronskian of these two homogeneous solutions is of course sinusoidal,

$$\mathcal{W}(\omega) = - [K \cos(KL) + \kappa \sin(KL)] . \quad (\text{A12})$$

If I assume that the observations are made above the cavity, $z > L$, as occurs for helioseismic observations, the Green's function has the solution

$$G(z, z'; \omega) = - \frac{\sin(Kz') \exp[-\kappa(z-L)]}{K \cos(KL) + \kappa \sin(KL)} . \quad (\text{A13})$$

Figure 5(a) shows the power spectrum and its components that result for this model when one assumes that the source is white (i.e., S_0 is constant),

$$P(\omega) = |S_0|^2 \frac{\sin^2(Kz') \exp[-2\kappa(z-L)]}{\mathcal{W}^2(\omega)} . \quad (\text{A14})$$

The effect of the height of observation, $\exp[-2\kappa(z-L)]$ (green curve), is a monotonically increasing function of frequency. The contribution from the Wronskian, $|\mathcal{W}|^{-2}$ (the red curve), behaves differently above and below the global cut-off frequency. Below the cut-off, a Lorentzian spike occurs at each mode frequency; above the cut-off, the Wronskian term oscillates and decays. The blue curve shows the driving efficiency, $\sin^2(Kz')$. It too is oscillatory, but with more rapid frequency variation than the Wronskian because $z' < L$. The zeros in the driving efficiency lead to the asymmetry in the total power profile (black curve).

In the alternate representation of a modal expansion, the Green's function and the power spectrum take on the form,

$$G(z, z'; \omega) = - \sum_{n=-N}^N \frac{K_n \kappa_n^2 c^4}{1 + \kappa_n L} \frac{\sin(K_n z') \exp[-\kappa_n(z-L)]}{\hat{\omega}_n \cos(K_n L)} \frac{1 - \delta_{n0}}{\omega - \omega_n} - \frac{1}{2\pi} \int_{C_{\text{BC}}} d\tilde{\omega} \frac{\sin(\tilde{K} z') \exp[\tilde{\kappa}(z-L)]}{\tilde{K} \cos(\tilde{K} L) + \tilde{\kappa} \sin(\tilde{K} L)} \frac{1}{\omega - \tilde{\omega}} , \quad (\text{A15})$$

$$P(\omega) = |S_0|^2 |G(z, z'; \omega)|^2, \quad (\text{A16})$$

where the eigenfrequencies ω_n (or equivalently Ω_n), wavenumbers K_n and evanescence rates κ_n are defined by the roots of the Wronskian, which provides a transcendental equation,

$$\mathcal{W}(\omega_n) \equiv -[K_n \cos(K_n L) + \kappa_n \sin(K_n L)] = 0, \quad (\text{A17})$$

$$K_n \equiv \frac{\Omega_n}{c}, \quad (\text{A18})$$

$$\kappa_n \equiv \frac{\sqrt{\alpha^2 - K_n^2 c^2}}{c}. \quad (\text{A19})$$

The wavenumber and evanescent length with the tilde, \tilde{K} and $\tilde{\kappa}$, are those corresponding to the integration frequency $\tilde{\omega}$, i.e., $\tilde{K} = K(\tilde{\omega})$ and $\tilde{\kappa} = \kappa(\tilde{\omega})$. Finally, the derivative of the Wronskian, evaluated at the mode frequencies, was used in these expressions,

$$\mathcal{W}'(\omega_n) = -\frac{\hat{\omega}_n}{c^4} \frac{1 + \kappa_n L}{K_n \kappa_n} \cos(K_n L). \quad (\text{A20})$$

Figure 5(b) shows the resultant power spectrum (thick black curve) as well as the power associated just with the modes P_{modes} (violet curve) and with the continuous spectrum P_{LW} (aqua curve),

$$P_{\text{modes}} = \left| \sum_{n=-N}^N \frac{K_n \kappa_n^2 c^4}{1 + \kappa_n L} \frac{\sin(K_n z') \exp[-\kappa_n(z - L)]}{\hat{\omega}_n \cos(K_n L)} \frac{1 - \delta_{n0}}{\omega - \omega_n} \right|^2, \quad (\text{A21})$$

$$P_{\text{LW}} = \frac{1}{4\pi^2} \left| \int_{C_{\text{BC}}} d\tilde{\omega} \frac{\sin(\tilde{K} z') \exp[\tilde{\kappa}(z - L)]}{\tilde{K} \cos(\tilde{K} L) + \tilde{\kappa} \sin(\tilde{K} L)} \frac{1}{\omega - \tilde{\omega}} \right|^2. \quad (\text{A22})$$

Similar to Figure 3, the thick orange curve shows the incoherent sum of the power in the modes,

$$P_{\text{inc}} = \sum_{n=-N}^N \left(\frac{K_n \kappa_n^2 c^4}{1 + \kappa_n L} \right)^2 \frac{\sin^2(K_n z') \exp[-2\kappa_n(z - L)]}{\hat{\omega}_n^2 \cos^2(K_n L)} \frac{1 - \delta_{n0}}{(\omega - \hat{\omega}_n)^2 + \gamma^2}. \quad (\text{A23})$$

REFERENCES

- Abrams, D. & Kumar, P. 1996, *ApJ*, 472, 882
- Basu, S. & Antia, H. M. 1999, *ApJ*, 525, 517
- Basu, S., Antia, H. M., & Bogart, R. S. 2001, in *Proc. SOHO 10/GONG 2000 Workshop: Helio- and Asteroseismology at the Dawn of the Millenium*, (ESA SP-464), 183
- Deubner, F. L. & Gough, D. 1984, *Ann. Rev. Astron. Astrophys.*, 22, 593
- Gabriel, M. 1992, *A&A*, 265, 771
- Gabriel, M. 1995, *A&A*, 299, 245
- Duvall, T. L., Jr., Jefferies, S. M., Harvey, J. W., Osaki, Y., & Pomerantz, M. A. 1993, *ApJ*, 410, 829
- Duvall, T. L., Jr., Harvey, J. W., Jefferies, S. M., & Pomerantz, M. A. 1991, *ApJ*, 373, 308
- Georgobiani, D., Stein, R. F., & Nordlund, Å. 2003, *ApJ*, 596, 698
- Jefferies, S. M., Severino, G., Moretti, P.-F., Oliviero, M., & Giebink, C. 2003, *ApJ*, 596, L117
- Korzennik, S. G. 2005, *ApJ*, 626, 585
- Kumar, P., Duvall, T. L., Jr., Harvey, J. W., Jefferies, S. M., Pomerantz, M. A., & Thompson, M. J. 1990, in *Proc. Oji Internat. Seminar*, eds. Y. Oskaki & H. Sibahashi (Berlin: Springer), 87
- Kumar, P. & Lu, E. 1991, *ApJ*, 375, L35
- Libbrecht, K. G. 1988, *ApJ*, 334, 510
- Nigam, R., Kosovichev, A. G., Scherrer, P. H., & Schou, J. 1998, *ApJ*, 495, L115
- Nigam, R. & Kosovichev, A. G. 1998, *ApJ*, 505, L51
- Nigam, R. & Kosovichev, A. G. 1999, *ApJ*, 514, L53
- Oliviero, M., Severino, G., Straus, Th., Jefferies, S.M., & Apporchaux, T. 1999, *ApJ*, 516, L45
- Rast, M. P. & Bogdan, T. J. 1998, *ApJ*, 496, 527

- Reiter, J., Rhodes, E. J., Kosovichev, A. G., Schou, J., & Scherrer, P. H. 2002, in *Proc. SOHO 11 Symposium. From Solar Min to Max: Half a Solar Cycle with SOHO*, (ESA SP-508), 87
- Rosenthal, C. S. 1998, *ApJ*, 508, 864
- Roxburgh, I. W. & Vorontsov, S. V. 1995, *MNRAS*, 272, 850
- Roxburgh, I. W. & Vorontsov, S. V. 1997, *MNRAS*, 292, L33
- Skartlien, R. & Rast, M. P. 2000, *ApJ*, 535, 464
- Toutain, T., et al. 1997, *Sol. Phys.*, 175, 311
- Toutain, T., Appourchaux, T., Frohlich, C., Kosovichev, A. G., Nigam, R., & Scherrer, P. H. 1997, *ApJ*, 506, L147
- Tripathy, S. C., Antia, H. M., Jain, K., & Hill, F. 2009, *ApJ*, 691, 365

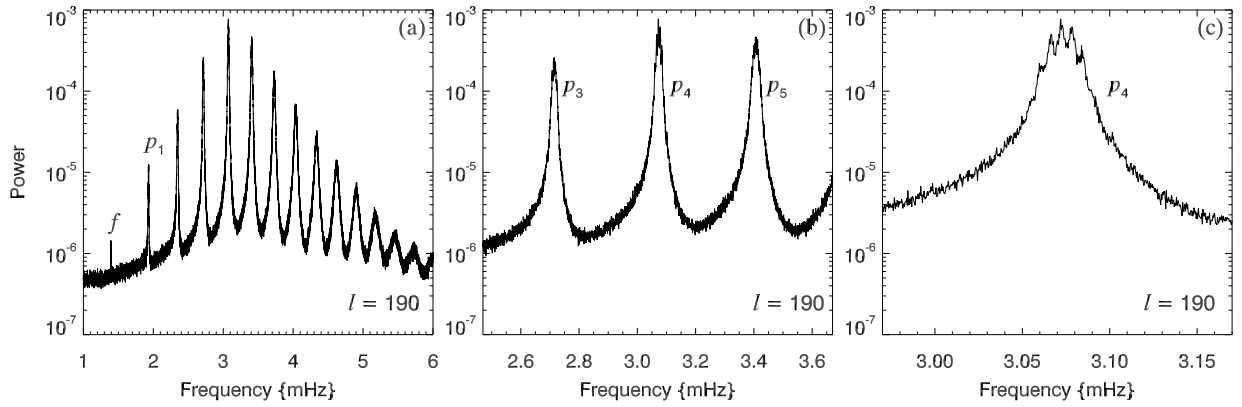


Fig. 1.— Power spectrum as a function of frequency for a harmonic degree of $l = 190$ and an azimuthal order of $m = 0$. The spectrum was calculated from Dopplergram data obtained by the GONG network. Ten years of data were separated into overlapping three month subintervals and the individual spectra for all subintervals were averaged together. The three panels show different frequency ranges around the p_4 mode. (a) The global context showing all of the ridges that exist below the acoustic cut-off frequency ($\nu_{ac} \approx 5.2$ mHz). (b) A narrower frequency range showing just the p_4 ridge and its nearest neighbors. (c) A narrow frequency band that demonstrates that the p_4 ridge is a blending of the $l = 190$, $n = 4$ mode and all of the spatial leaks from modes of nearby harmonic degree. Differences in degree up to ± 2 are clearly visible. The frequency profile of the blended line profiles are obviously skewed or asymmetric.

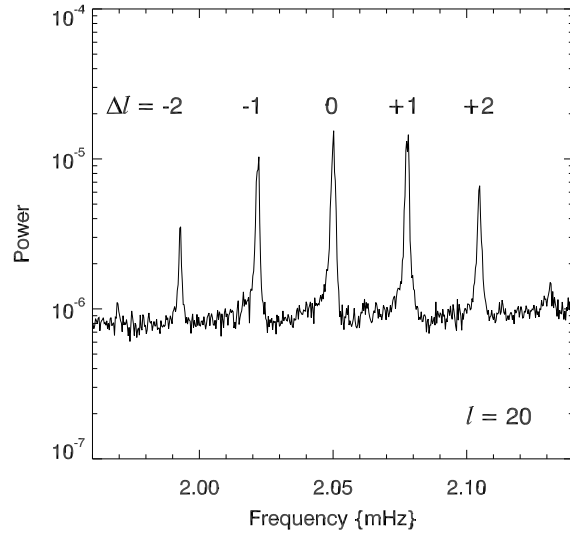


Fig. 2.— Power spectrum as a function of frequency for waves with $l = 20$ and $m = 0$. The same data as in Fig. 1 were used. For low values of harmonic degree (as illustrated here), each mode peak is well-separated from the spatial leaks of nearby modes. The leaks from modes degrees up to ± 2 are shown here. Each of the frequency profiles (for the target mode as well as the leaks) is skewed and asymmetric.

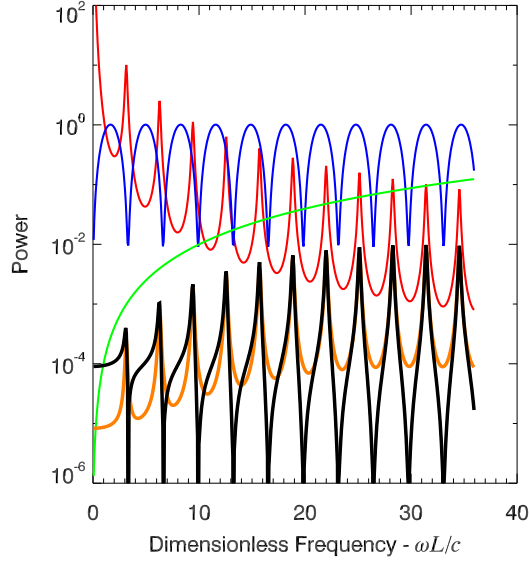


Fig. 3.— The power spectrum for our simple “guitar-string” model. The source height is $z' = 0.95 L$ and the observation height is at $z = 0.99 L$. The damping time is small compared to the sound-crossing time, $\gamma L/c = 0.1$. The thick black curve shows the power spectrum of the solution as a function of frequency, and can be represented in either of two equivalent ways, equation (2.17) or (3.12). The thin colored curves show the contributions from three separate factors in equation (2.17): the effect of the height of observation (green curve), the reciprocal of the square of the Wronskian (red curve), and the driving efficiency (blue curve). The total power is the product of these three factors. The Wronskian embodies the modal structure, and everywhere there is a resonant mode frequency the Wronskian vanishes, providing a peak with a Lorentzian profile. The driving efficiency possesses zeros at frequencies lying between the modes. Asymmetry arises because the zeros of the driving efficiency do not fall symmetrically between the mode frequencies. An alternative interpretation is that the modes represented in equation (3.12) interfere with each other to produce the asymmetry. The thick orange curve demonstrates that the line profiles becomes symmetric if one neglects mode interference and assumes that the total power is the incoherent sum of the power in all modes.

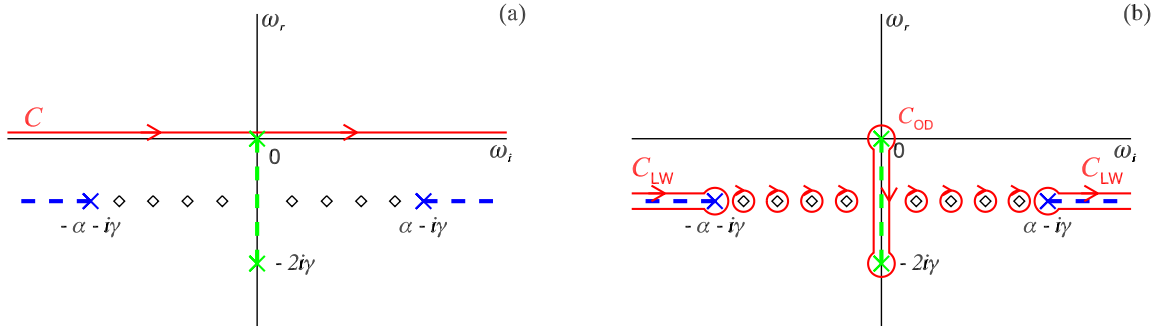


Fig. 4.— Complex frequency space through which the inverse Fourier transform integral is performed. (a) The integration contour (red line labeled C) originally lies along the real frequency axis. (b) For $t > 0$, the contour is deformed downwards and picks up contributions from each of the singularities. The diamonds mark the location of the poles of the Green’s function, which correspond to the acoustic cavity’s complex mode frequencies. The green crosses denote the branch points that frame the branch cut (green dashed line) associated with overdamped waves. The integration contour around this branch cut is shown in red and labeled C_{OD} . The branch points and cut associated with leaky waves are indicated in blue, and the contour around this branch cut is labeled C_{LW} .

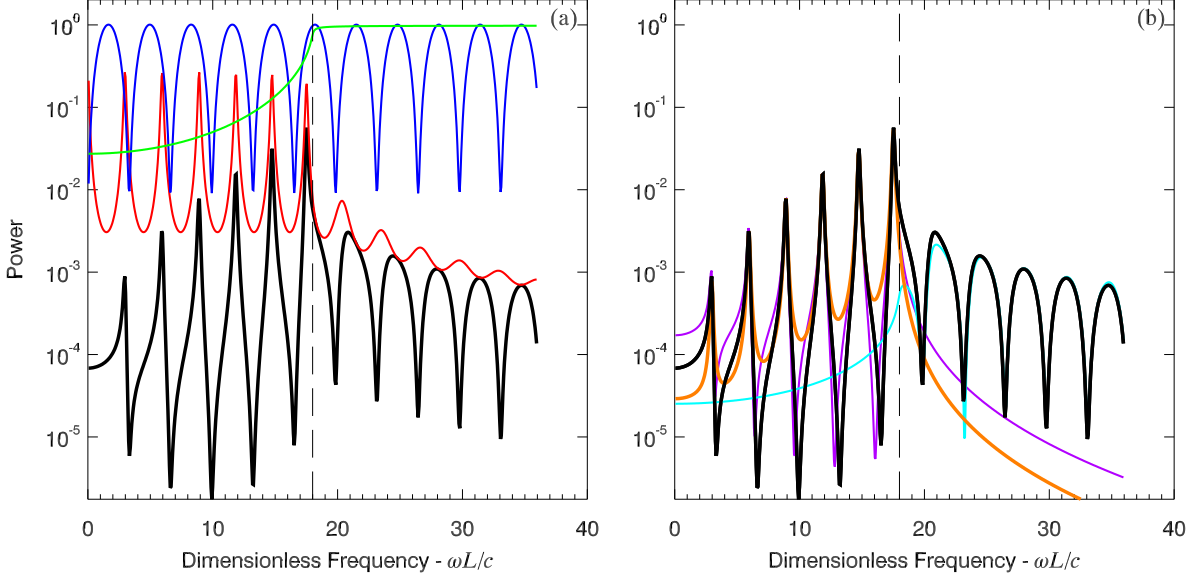


Fig. 5.— The power spectrum for an acoustic cavity corresponding to a leaky square-well potential with a cavity depth of L . The source height is $z' = 0.95 L$, the global cut-off frequency is chosen to be $\alpha = 18.0 c/L$, and the damping parameter is the same as in Figure 3, $\gamma = 0.1 c/L$. The observation height is at $z = 1.1 L$, just above the upper boundary of the cavity. (a) The thick black curve shows the power spectrum as a function of frequency obtained through equation (A14). The colored curves have the same meaning as in Figure 3. The vertical dashed line indicates the global cut-off frequency α . Asymmetry arises because the zeros of the driving efficiency (blue curve) do not fall symmetrically between the mode frequencies. (b) The power spectrum (thick black curve) obtained through an eigenfunction expansion, equation (A16). The violet curve shows the power associated with just the modes, P_{modes} , and the aqua curve shows the power due to the continuous spectrum of leaky waves, P_{LW} . The thick orange curve presents the incoherent sum of the power in the modes, P_{inc} . The asymmetry apparent in the power is the result of interference between modes and between modes and the leaky waves.